TM-2249

COHERENT PARASITIC ENERGY LOSS OF THE RECYCLER BEAM

K.Y. Ng

Fermi National Accelerator Laboratory, P.O. Box 500, Batavia, IL 60510*

(May, 2004)

Abstract

Parasitic energy loss of the particle beam in the Recycler Ring is discussed. The long beam confined between two barrier waves has a spectrum that falls off rapidly with frequency. Discrete summation over the revolution harmonics must be made to obtain the correct energy loss per particle per turn, because only a few lower revolution harmonics of real part of the longitudinal impedance contribute to the parasitic energy loss. The longitudinal impedances of the broadband rf cavities, the broadband resistive-wall monitors, and the resistive wall of the vacuum chamber are discussed. They are the main sources of the parasitic energy loss.

*Operated by the Universities Research Association, Inc., under contract with the U.S. Department of Energy.

1 INTRODUCTION

For a coasting beam, the arrival time of a beam particle at a designated point of the accelerator ring is random. The energy loss of the beam particle becomes incoherent so that the loss per particle is independent of the beam intensity. [1] The image current of the individual particle is short and is of the order $\sim b/\gamma$ where b is the radius of the vacuum chamber and γ is the ratio of the particle's energy to the particle's rest energy. The parasitic energy loss at the discontinuities of the vacuum chamber therefore samples the high frequency part of the impedance of vacuum chamber. The beam inside the Recycler Ring is stored between two barrier waves. It is long but is not coasting. The arrival time of a beam particle is no longer random. The energy loss of the beam is dominated by its coherent effect, so that the loss per particle is proportional to the intensity of the beam. For the long beam, the spectrum falls off rapidly with frequency and, in general, only a few lower revolution harmonics are significant. Thus only the very low-frequency part of the impedance of the vacuum chamber contributes to the parasitic energy loss.

In this paper, we first derive the expression for coherent parasitic energy loss. Since only very few lower revolution harmonics contribute and the real part of the longitudinal impedance vanishes at zero frequency, the usual integral representation of the energy loss overestimates the loss and we must stick to summation over harmonics instead.

We next discuss the various elements in the vacuum chamber of the Recycler Ring that give the largest contribution to the real part of the longitudinal impedance at low frequencies. We find that most of the contribution comes from the four broadband rf cavities. The broadband resistive-wall monitor that has a 25-Ω resistor across the gap also contributes, although not as much as the rf cavities. The contribution of the resistive wall of the vacuum chamber is also included. The loss for each item and the total loss are computed as functions of the distance between the two barrier waves that contain the beam.

2 PARASITIC ENERGY LOSS

2.1 NON-PERIODIC EXPRESSION

For a particle in a bunch with arrival time advance τ relative to the synchronous particle,

the energy *gain* experienced in a revolution turn is

$$\mathcal{E}(\tau) = -e^2 N \int_{\tau}^{\hat{\tau}} d\tau' \lambda(\tau') W_0'(\tau' - \tau) \ , \tag{2.1}$$

where $\lambda(\tau)$ is the linear density of the bunch normalized to unity and $W_0'(\tau' - \tau)$ is the longitudinal monopole wake experienced by the test particle coming from a beam particle with arrival time advance τ'. The upper limit of integration $\hat{\tau}$ is the arrival time advance of the head of the bunch and it can be extended to infinity if the wake is shorter than the gap between bunches. The lower limit can also be extended to $-\infty$ because of the causal behavior of the wake. The negative sign in front implies that the particle actually experiences an energy loss. Expressed in terms of the longitudinal monopole impedance $Z_0^{\parallel}$ using

$$W_0'(\tau) = \frac{1}{2\pi} \int_{-\infty}^{\infty} d\omega \, Z_0^{\parallel}(\omega) e^{-i\omega\tau} \ , \tag{2.2}$$

and the Fourier transform of the linear density

$$\tilde{\lambda}(\omega) = \frac{1}{\sqrt{2\pi}} \int_{-\infty}^{\infty} d\tau \, \lambda(\tau) e^{-i\omega\tau} \ , \tag{2.3}$$

the energy loss per turn becomes

$$\mathcal{E}(\tau) = -\frac{e^2 N}{\sqrt{2\pi}} \int_{-\infty}^{\infty} d\omega \, \tilde{\lambda}(\omega) Z_0^{\parallel}(\omega) e^{i\omega\tau} \ . \tag{2.4}$$

We see that particles at different arrival time advance lose energy differently. If we average over all the particles in the bunch, the average energy gain per turn is

$$\bar{\mathcal{E}} = \int_{-\infty}^{\infty} d\tau \lambda(\tau) \mathcal{E}(\tau) = -e^2 N \int_{-\infty}^{\infty} d\omega \left| \tilde{\lambda}(\omega) \right|^2 Z_0^{\parallel}(\omega) \ . \tag{2.5}$$

Notice that

$$\begin{aligned} \left| \tilde{\lambda}(\omega) \right|^2 &= \frac{1}{2\pi} \int_{-\infty}^{\infty} d\tau \int_{-\infty}^{\infty} d\tau' \lambda(\tau) \lambda(\tau') e^{-i\omega(\tau - \tau')} \\ &= \frac{1}{2\pi} \int_{-\infty}^{\infty} d\tau \int_{-\infty}^{\infty} d\tau' \lambda(\tau) \lambda(\tau') \cos[\omega(\tau - \tau')] \ , \end{aligned} \tag{2.6}$$

because the expression is real. Thus $|\tilde{\lambda}(\omega)|^2$ is symmetric in ω. Therefore only $\mathcal{R}e \, Z_0^{\parallel}$ contributes in Eq. (2.5).

2.2 PERIODIC EXPRESSION

The Fourier transform of the linear density has not been performed correctly. When synchrotron motion is neglected, the linear density λ as a function of arrival time advance τ is periodic in τ with period $T_0 = 2\pi/\omega_0$. The Fourier transform is therefore discrete. The expansion is

$$\lambda(\tau) = \frac{\sqrt{2\pi}}{T_0} \sum_{n=-\infty}^{\infty} \tilde{\lambda}_n e^{in\omega_0\tau} \ . \tag{2.7}$$

Instead of Eq. (2.3), the transform is

$$\tilde{\lambda}_n = \frac{1}{\sqrt{2\pi}} \int_{-T_0/2}^{T_0/2} d\tau \, \lambda(\tau) e^{-in\omega_0\tau} \ . \tag{2.8}$$

$$\mathcal{E}(\tau) = -\frac{e^2 N\omega_0}{\sqrt{2\pi}} \sum_{n=-\infty}^{\infty} \lambda_n Z_0^{\parallel}(n\omega_0) e^{in\omega_0\tau} \ . \tag{2.9}$$

$$\bar{\mathcal{E}} = -e^2 N\omega_0 \sum_{n=-\infty}^{\infty} \left|\tilde{\lambda}(\omega)\right|^2 \mathcal{R}e \, Z_0^{\parallel}(\omega) \ . \tag{2.10}$$

An unconventional constant has been placed in front of the summation in the harmonic expansion of Eq. (2.7) so that the discrete Fourier transform $\tilde{\lambda}_n$ of Eq. (2.8) has similar definition as the non-periodic transform $\tilde{\lambda}(\omega)$ of Eq. (2.3). This also results in the average energy loss expression very similar to the corresponding non-periodic one. In fact, one can translate the non-periodic expressions to the periodic ones by just substituting

$$\begin{cases} \tilde{\lambda}(\omega) \longrightarrow \tilde{\lambda}_n \\ \displaystyle\int_{-\infty}^{\infty} d\omega \longrightarrow \omega_0 \sum_{n=-\infty}^{\infty} \end{cases} \tag{2.11}$$

When the bunch is short, there is not much difference between Eqs. (2.5) and (2.10), because the spectrum of the bunch extends to very high frequencies and therefore many harmonics. However, for very long bunches, especially those in the Recycler, where a bunch may occupy over 80% of the ring, the difference becomes very large, because there are only very few low harmonics that contribute. For a bunch of length τ_0 with sharp edges with distribution

$$\lambda(\tau) = \begin{cases} \dfrac{1}{\tau_0} & |\tau| < \frac{\tau_0}{2} \\ 0 & \text{otherwise} \ , \end{cases} \tag{2.12}$$

the power spectrum is

$$\left|\tilde{\lambda}_n\right|^2 = \frac{1}{2\pi}\left(\frac{\sin n\omega_0\tau_0/2}{n\omega_0\tau_0/2}\right)^2 , \tag{2.13}$$

for all n from $-\infty$ to $+\infty$. Let us look at the lower harmonics. The zero harmonic does not contribute because $\mathcal{R}e\, Z_0^{\|}(0) = 0$. At the other low harmonics, the argument of sine,

$$\frac{n\omega_0\tau_0}{2} = n\pi\frac{\tau_0}{T_0} \tag{2.14}$$

is close to $n\pi$ if the bunch length is nearly as long as the circumference of the ring. Thus, the energy loss per turn will be very small. For example, if $\tau_0/T_0 = 0.82$, $|\tilde{\lambda}_n|^2 = 0.00689$, 0.00491, 0.00262, 0.00089, $\cdots$, respectively, for $n = \pm1$, ±2, ±3, ±4, $\cdots$, indicating that only a few low harmonics are important. On the other hand, if the non-periodic expression of Eq. (2.5) is used instead, the large $\sin x/x$ peak will have been partially included, even with a $\mathcal{R}e\, Z_0^{\|}$ that goes to zero at zero frequency.

Let us employ the longitudinal impedance of one of the rf cavities in the Recycler Ring. The real part has been measured by Wildman [2] and is depicted in Fig. 4 as black dots. The average energy loss of a particle per revolution turn subject to one rf cavity is computed at different full bunch length τ_0, and is depicted as solid in Fig. 1. The bunch is assumed to have sharp edges. The approximated solution using integration rather than summation is also shown in the same figure as dashes. We see that the energy loss decreases to zero as soon as the bunch fills the whole circumference of the Recycler Ring ($\tau_0 = T_0 =$ 11.13 μs), while the approximation using integration gives nonzero energy loss. This clearly indicates that discrete summation is important because only a few low harmonics of the power spectrum contribute. The difference between the two computations decreases as the bunch length becomes shorter, because many harmonics have to be used to describe the bunch and therefore the integration is a good approximation of the discrete summation.

The energy loss expressions derived above are for *coherent* energy loss, implying that only the loss due to the coherent spectrum has been taken into account. This can be understood by realizing that we have been referring to the power spectrum of a bunch but not the spectrum of the individual particles. For this reason, the total energy loss by the bunch is proportional to N^2 and the per particle energy loss is proportional to N. If we start off with the spectra of the image currents of individual beam particles, we will find that each of them carries a phase corresponding to the time of arrival at some designating point of the ring. For a very short bunch, these current spectra add coherently giving the same energy loss as our computation above. When the bunch fills up the whole ring, the

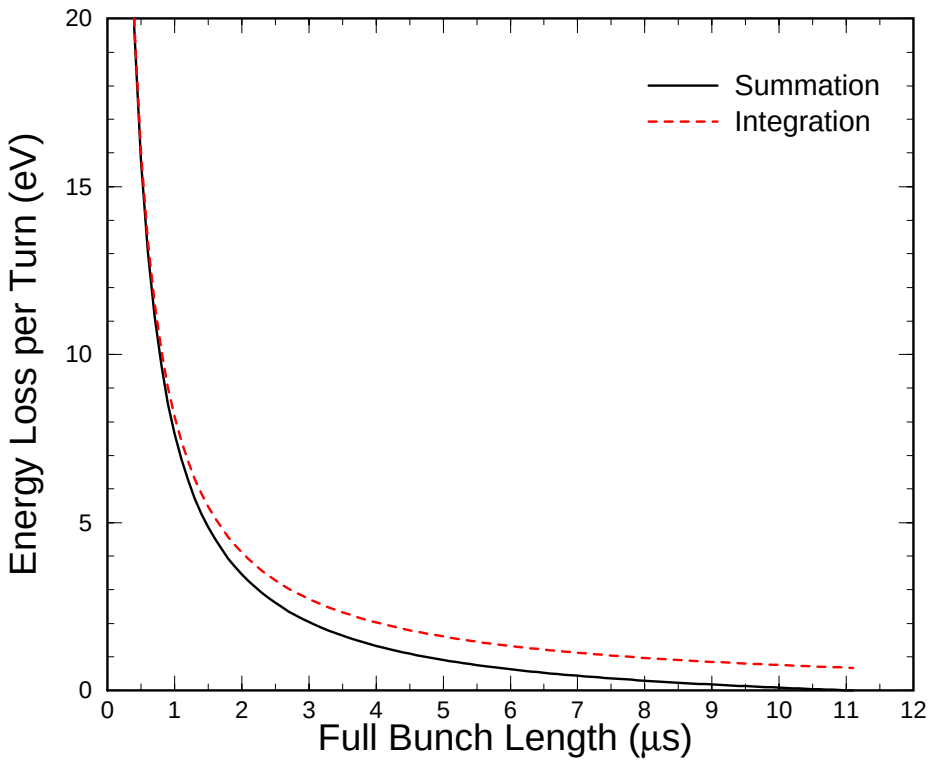

Figure 1: Energy loss of a particle in a sharp-edge bunch per turn subject to a Recycler rf cavity is shown as a function of total bunch length τ_0. The exact calculation using discrete summation over harmonics is shown in solid, while the integration-approximated calculation is shown in dashes.

beam becomes coasting and the phase of the image current spectrum becomes random. The incoherent signals of the beam lead to an energy loss per particle per turn of

$$\mathcal{E} = -\frac{e^2}{\pi} \int_0^\infty \frac{\mathcal{R}e\, Z_0^{\|}(\omega)}{I_0(x)^2} \ , \tag{2.15}$$

where $I_0(x)$ is the modified Bessel function of order zero and $x = \omega b/(\gamma\beta c)$, in which b is beam pipe radius, c the velocity of light and γ and β the relativity parameters of the beam. It will be more accurate if we replace the integration by summation over the revolution harmonics. However, this replacement is not necessary because $1/I_0(x)^2$, the power spectrum of the image current of a beam particle, extends to very high frequencies. (It rolls to one half at 11 GHz for a $b = 5$ cm beam pipe.)

2.2.1 Beam in a Barrier Bucket

For a beam confined between two barrier waves with barrier voltage $\pm V_0$, the Hamiltonian describing the motion of a beam particle is

$$H = \frac{|\eta|\Delta E^2}{2\beta^2 E} + \frac{eV_0}{T_0}\left(\tau - \frac{\tau_0}{2}\right)\Theta \qquad \text{with } \Theta = \begin{cases} 0 & |\tau| < \frac{1}{2}\tau_0 \\ 1 & |\tau| > \frac{1}{2}\tau_0 \end{cases} \tag{2.16}$$

where the arrival time advance τ and energy offset ΔE have been chosen as the canonical variables and time is the independent variable. The barriers are placed at $|\tau| > \frac{1}{2}\tau_0$ and η is the slip parameter. For a maximum energy offset $\widehat{\Delta E}$, the penetration into the barrier is easily found to be

$$\Delta\tau = \frac{|\eta| T_0 \widehat{\Delta E}^2}{2\beta^2 E e V_0} \ . \tag{2.17}$$

For convenience let us define

$$\sigma_\tau = \frac{|\eta| T_0 \sigma_E^2}{2\beta^2 E e V_0} \ . \tag{2.18}$$

as the penetration of a particle with energy offset σ_E.

For long-time storage, the energy distribution should become Gaussian, or the longitudinal phase-space distribution is

$$\psi(\tau, \Delta E) \propto \exp\left(-\frac{\beta^2 E}{|\eta|\sigma_E^2} H\right) \ , \tag{2.19}$$

where σ_E is the rms energy spread. After integrating over the energy offset, we obtain the linear particle density

$$\lambda(\tau) = \lambda(0) \exp\left[-\frac{\left(\tau - \frac{1}{2}\tau_0\right)}{2\sigma_\tau}\Theta\right] \ . \tag{2.20}$$

To normalize $\lambda(\tau)$ to unity, we find

$$\frac{1}{\lambda(0)} = \tau_0 + 4\sigma_\tau\left(1 - e^{-\widehat{\Delta E}^2/\sigma_E^2}\right) \tag{2.21}$$

Since $\widehat{\Delta E} \approx 3\sigma_E$ in general, the exponential can be neglected. The Fourier transform can be readily performed to give

$$\tilde{\lambda}(\omega) = \frac{2\lambda(0)}{\sqrt{2\pi}}\left[\frac{\sin\frac{1}{2}\omega\tau_0}{\omega} + 2\sigma_\tau \frac{\cos\frac{1}{2}\omega\tau_0 - 2\omega\sigma_\tau \sin\frac{1}{2}\omega\tau_0}{1 + 4\omega^2\sigma_\tau^2}\right] \tag{2.22}$$

Energy loss of a particle per turn in a beam inside a barrier bucket subject to a Recycler rf cavity is shown as a function of barrier separation τ_0. The total bunch length is the sum of τ_0 and the penetrations into the barriers on both sides. Now energy loss depends on energy offset also, because of barrier penetration. The exact calculation using discrete summation over harmonics is shown in Fig. 2 for rms energy offset σ_E = 0, 3, 6, and 9 MeV. We see

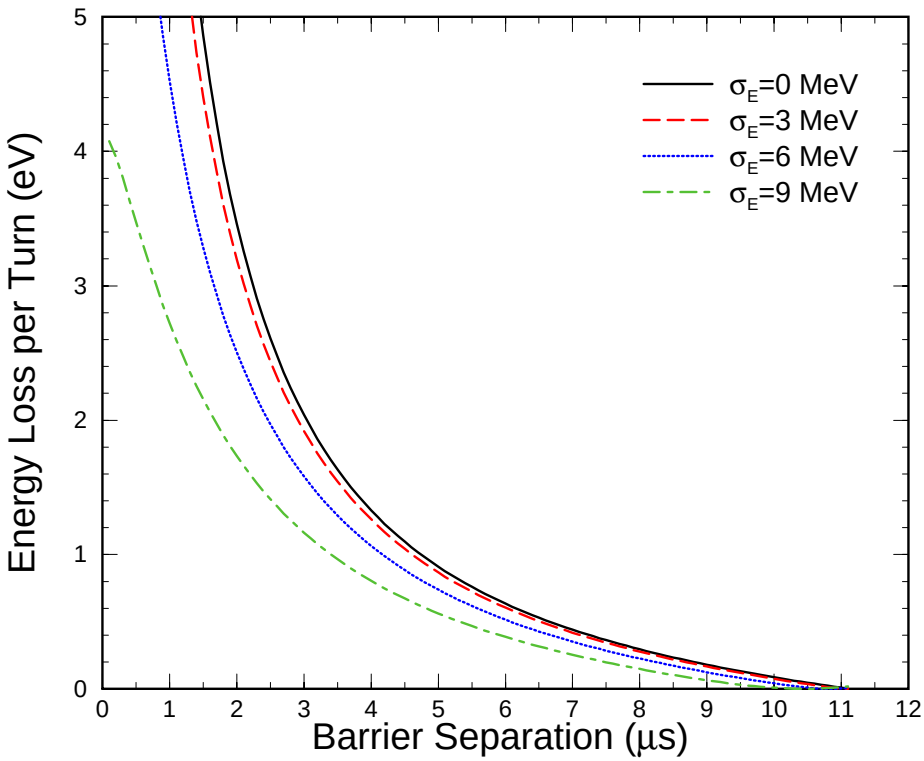

Figure 2: Coherent energy loss of a particle per turn in beam confined by two barrier waves is shown as functions of barrier separation τ_0 for rms energy spread σ_E = 0, 3, 6, and 9 MeV. The impedance is contributed by a broadband rf cavity of the Recycler Ring. Discrete summation over harmonics has been employed. .

that when the bunch is short, the dependence on energy offset is more evident, because penetrations into the barriers have become a more important part of the total bunch length. On the other hand, the dependence on energy offset is much less when the bunch is long. At $\tau_0 = 9.3$ μs, the average loss of energy per particle per turn is 0.151, 0.138, 0.098 eV for σ_E = 0, 3, and 6 MeV. Here the measured impedance of one rf cavity, as depicted in Fig. 4 has been used. By the way two 1-μS barriers of width 1 μs and barrier voltages ± 2 kV can hold a Recycler beam with maximum energy offset $\widehat{\Delta E} = 18.4$ MeV or $\sigma \approx 6.1$ MeV.

3 IMPEDANCE OF RECYCLER RING

3.1 RF CAVITIES

A schematic drawing of a cavity is shown in Fig. 3. The are four 50 Ω broadband

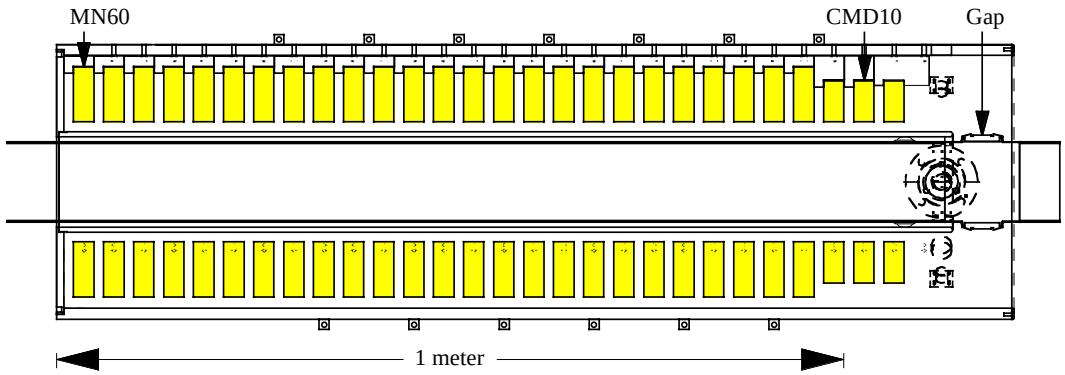

Figure 3: Schematic drawing of a Recycler wideband rf cavity, showing the 24 MN60 ferrite cores, the 3 CMD10 ferrite cores, and the gap at the right side.

ferrite-loaded rf stations [2]. The amplifiers are of 3.5 kW from 10 kHz to 100 MHz, capable of supplying a total of ±2 kV. The rf waveform generated is determined by the amplitude and phase of each of the 588 revolution harmonics.

A station consists of a 12.5″ diameter water-cooled outer aluminum shell, a 5″ diameter aluminum inner conductor, and a 4″ diameter stainless steel beam pipe with a 1″ ceramic gap which is electrically connected to the cavity with beryllium-copper finger stock. The cavity is filled with 25 11.5″ OD by 6″ ID by 1″ thick Mn-Zn ferrite cores (MN60) and three 10″ OD by 6″ ID by 1″ thick Ni-Zn ferrite cores (CMD10). The ferrite cores are air-cooled, spaced by 0.5″, and supported by Kapton spacer blocks. A 60 Ω resistor is connected directly across the cavity gap and to the inner conductor at the gap by 1″ wide by 4″ long copper straps.

The outer and inner aluminum shells form a ferrite loaded coaxial transmission line. The impedance seen by a particle beam consists of the 60 Ω resistor and the copper strap in parallel with the input impedance of the coaxial transmission line. According to the specification, the ferrite cores have magnetic permeabilities $\mu_r' = 6500$ (MN60) and 550 (CMD10) at low frequencies, while their dissipative components μ_r'' peak at ~ 10 MHz. The

simplest representation of the magnetic property of a ferrite core is a resistor R and an inductor L in parallel, giving

$$\mu_r' - j\mu_r'' = [\mu_r']_{\omega=0} \frac{1 - j\omega/\omega_r}{1 + \omega^2/\omega_r^2} \ , \tag{3.1}$$

where $\omega_r = L/R$ and $[\mu_r']_{\omega=0}$ is μ_r' at zero frequency. For our ferrite cores, we set $\omega_r/(2\pi) =$ 10 MHz. The inductance L is inferred via the inductance of the ferrite cores at low frequencies. The capacitance of the coaxial line can be computed easily by assuming that the relative electric permittivity of the ferrite cores is $\epsilon_r = 10$. Notice that there is a lot of empty space inside the coax and this must be taken into account in the computation of the capacitance. On the other hand, the air space can be neglected in the computation of inductance because of the very large permeability of the ferrite cores. The result of the computation is shown in Fig. 4.

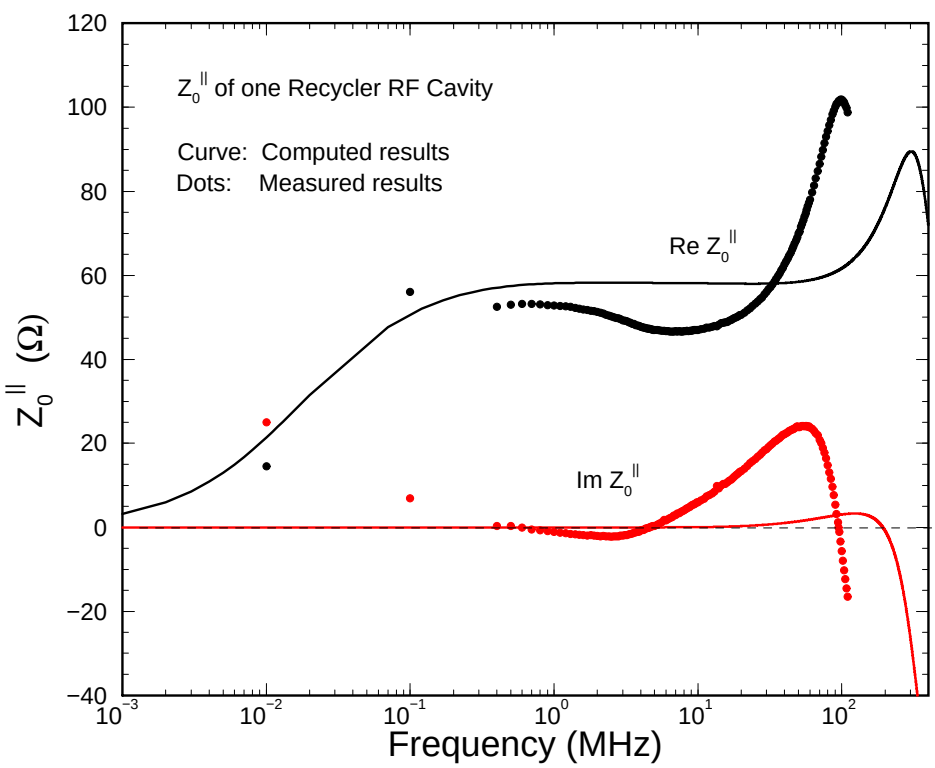

Figure 4: $Re Z_0^{\parallel}$ and $\mathcal{I}m\, Z_0^{\parallel}$ of a rf cavity in the Recycler Ring computed as the resistor across the gap in parallel with the input impedance of a coaxial transmission line. Measurement by Wildman is also shown as circular dots.

The impedance experienced by the beam can be understood as follows. At very low frequencies, the image current flows through the inner aluminum shell to the end of the

coaxial line and return through the outer aluminum shell. Thus the impedance is almost zero. As the frequency increases, the image current will find it harder and harder to flow through the aluminum shells because of the inductance of the ferrite cores. As the input impedance of the coaxial line increases, the image current will find it easier to flow through the 60 Ω resistor across the gap instead. In order that the impedance seen by the beam increases to 60 Ω at 100 kHz, a lot of ferrite cores are therefore required. In general, we are satisfied with the comparison of the computed $Z_0^{\|}$ with the measurement by Wildman, except for $\mathcal{I}m\, Z_0^{\|}$ below $\sim$ 300 MHz. It is not easy to understand why the measured data become so much inductive. The trend of the computed $Z_0^{\|}$ at high frequencies follows that of measurement. However, both measured $\mathcal{R}e\, Z_0^{\|}$ and $Z_0^{\|}$ start to roll off at much lower frequencies than the computed results. This may be due to the very crude ferrite model that we used in Eq. (3.1). Some more remarks about the computation are listed below:

1. We find that the strap, that is in series of the 60 Ω resistor across the gap, plays an important role in the rising of both $\mathcal{R}e\, Z_0^{\|}$ and $Z_0^{\|}$ at high frequencies. In the calculation the strap is considered as a 32-nH inductor.†

2. The termination of the coaxial line is important to the impedance experienced by the beam at low frequencies This is because this termination resistor in parallel with the 60 Ω resistor across the gap is what the beam sees at low frequencies. In the calculation, the termination resistor has been considered to be zero (or the line shorted). A small inductance at the termination will not affect the result at all.

3. The relative electric permittivity (or dielectric constant) of the ferrite cores is important to the input impedance of the coaxial transmission line, but is unimportant to the impedance seen by the beam. This is because, at low frequencies, capacitance effect of the ferrite cores is of no importance, and at high frequencies, the image current mostly flows through the resistor of the gap instead of the coaxial line containing the ferrite.

4. We have also included the wall resistivity of the aluminum shells and found that its contribution is too small to affect anything.

5. The gap is connected by a metallic strap($\sim$ 32 nH) to the inner conductor of a cable leading to the amplifier which has a load of 50 Ω. Therefore what the particle sees is

†The strap forms a transmission line with the surrounding with characteristic impedance $Z_c = \sqrt{L/C}$ and velocity $v = 1/sqrtLC$, where L and C are, respectively, the inductance and capacitance per unit length. Thus the inductance of the strap of length $\ell = 3.75''$ is $L\ell = Z_c\ell/v \sim 32$ nH, assuming $Z_c \sim 100$ Ω and $v \sim$ velocity of light. Acknowledgment is given to J. Crisp for the estimation.

what we calculated before in parallel with this 50 Ω plus 32 nH. There are 4 such rf cavities in total. The energy loss per turn of the beam to these cavities is computed when the beam has rms energy spread of 3 MeV and intensity 100×10^{10}. The result is plotted in Fig. 5.

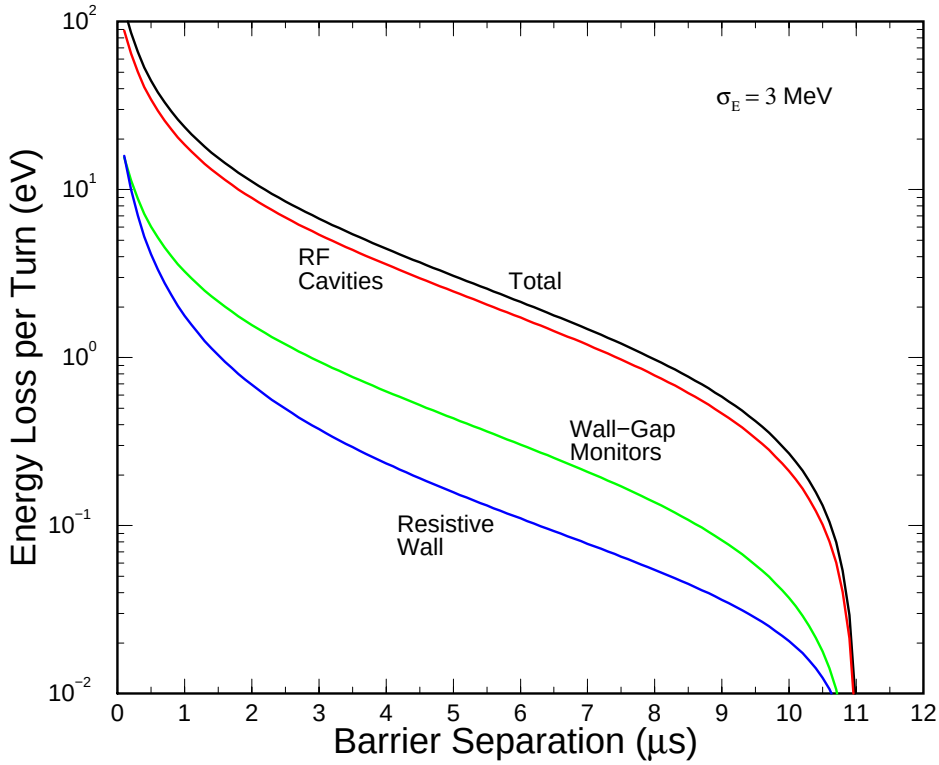

Figure 5: For a particle beam of rms energy spread 3 MeV and intensity 100×10^{10}, the energy loss per particle per turn is shown individually for the rf cavities, the resistive-wall monitors, and the resistive wall.

3.2 RESISTIVE WALL MONITOR

The resistive wall monitor is very similar to the rf cavity in structure. The cavity gap is replaced here with a 140-mil narrow annular piece of ceramic. The image current flows across the gap through about 100 resistors at the outer circumference of the ceramic. The voltages across these resistors are then sampled at 4 locations, combined, and directed to the analyzer. The combined resistance of these 100 resistors is about 1 Ω, which the particle beam is experiencing. In order that the image current will flow through these resistors even

at frequencies as low as 3 kHz instead of flowing through the outer metallic can, a number of ferrite cores are placed inside the metallic can. There must be enough ferrite cores so that they have an impedance of $\sim 30\ \Omega$ at 3 kHz. This will ensure that the error in the voltage across the resistors at the gap is less than 3.3% when the frequency is low. Thus similar to the rf cavity, the resistive wall monitor will contribute $\mathcal{R}e\, Z_0^{\parallel} \sim 1\ \Omega$ from 3 kHz to 6 GHz with $\mathcal{I}m\, Z_0^{\parallel}$ very much smaller.

There is a special resistive wall monitor which has a combined gap resistance of 25 Ω in roughly the same frequency range. Because of the much larger gap resistance, more image current will flow through the shielding can instead. Thus this monitor will be much less accurate than the one with only 1-Ω gap resistance. This monitor is used mostly as a longitudinal kicker, for example, in stochastic cooling.

A simple circuit model for the impedance seen by the beam is a resistor in parallel with an inductor. Mathematically, this impedance can be expressed as

$$Z_0^{\parallel}\Big|_{\text{wall-gap}} = R_{\text{gap}} \frac{j + \omega/\omega_r}{1 - \omega^2/\omega_r^2}\ , \tag{3.2}$$

where $\omega_r/(2\pi) = 3$ kHz and $R_{\text{gap}} = 1$ or 25 Ω for the two different monitors. The energy loss per turn per particle from these two monitors is computed. The result is shown in Fig. 5 when the beam has a rms energy spread of 3 MeV and intensity 100×10^{10}.

3.3 RESISTIVE-WALL IMPEDANCE

The Recycler Ring has an elliptical beam pipe of major and minor diameters 3.806″ and 1.75″. If we take the average and let $b = 3.528$ cm be the radius of the effective cylindrical approximate, the real part of the wall impedance of the beam pipe is

$$\mathcal{R}e\, Z_0^{\parallel}\Big|_{\text{BPM}} = \frac{1}{b}\sqrt{\frac{Z_0 \rho R \beta}{2}} = 7.580\ \Omega \tag{3.3}$$

where stainless steel resistivity $\rho = 7.4 \times 10^{-7}$ Ωm has been used. When this is substituted into Eq. (2.10) with the discrete spectrum of the beam given in Eq. (2.22), the energy loss per turn per particle can be computed. The result is shown in Fig. 5 when the beam has a rms energy spread of 3 MeV and intensity 100×10^{10}.

Other elements in the vacuum chamber like the pump ports, bellows, beam-position monitors (BPMs), etc have their real parts of the impedance increasing slowly as ω^2 and

reaching peaks or resonances at hundreds of MeV. They therefore contribute negligibly to the energy loss of the long Recycler beam. As an example, approximating the split-can BPMs as cylindrical strip lines of length $\ell = 12''$ with covering angle $\phi \approx \pi$, the real part of the impedance is

$$\mathcal{R}e\, Z_0^{\parallel}\Big|_{\rm BPM} = 2MZ_c \left(\frac{\phi}{2\pi}\right)^2 \sin^2 \frac{\omega\ell}{c}\ , \tag{3.4}$$

where $Z_c = 50\ \Omega$ is the termination impedance. We see that $\mathcal{R}e\, Z_0^{\parallel}\big|_{\rm BPM}$ increases as ω^2 and reaches its first maximum at 182.5 MHz. For $M = 410$ BPMs, we get $\mathcal{R}e\, Z_0^{\parallel}\big|_{\rm BPM} = 0.0034\ \Omega$ at the revolution frequency. Thus the BMPs contribute negligibly as compared with the rf cavities.

4 CONCLUSIONS

We have analyzed the coherent parasitic energy loss of the Recycler beam. The contribution comes from the low-frequency part of the impedance of the Recycler vacuum chamber. The elements that give the most contribution are the rf cavities and resistive-wall monitors, because they are broadband starting from very low frequencies, 100 kHz for the rf cavities and 3 kHz for the resistive-wall monitors. A small contribution comes from the wall resistivity of the vacuum chamber with the impedance increasing as $\sqrt{\omega}$ at low frequencies. Other elements, like the BPMs, pump ports, etc, contribute negligibly, because the real part of their impedances increases slowly as ω^2 at low frequencies and reaches peaks or resonances at hundreds of MeV.

The coherent parasitic energy loss per particle per turn for each element is computed as a function of separation of the two barrier waves that confine the Recycler beam. The total energy loss per particle of a beam of intensity 100×10^{10} is depicted in Fig. 6 at several rms energy spreads. In the computation, we cannot just integrate over frequency. Instead, one must sum over revolution harmonics. This is because the impedance vanishes at zero frequency and only a few low harmonics contribute. The coherent per particle energy loss computed must be compensated by shifting the potential baseline between the barriers by the same amount, otherwise a slant will appear in the linear density of the beam [3]. In Ref. [3], the compensation was computed via the multiplication of the local beam current by a constant $\mathcal{R}e\, Z_0^{\parallel}$, and the result appeared to be systematically larger than what was needed experimentally. Hopefully, a discrete summation over the revolution harmonics will produce the more accurate compensation voltage.

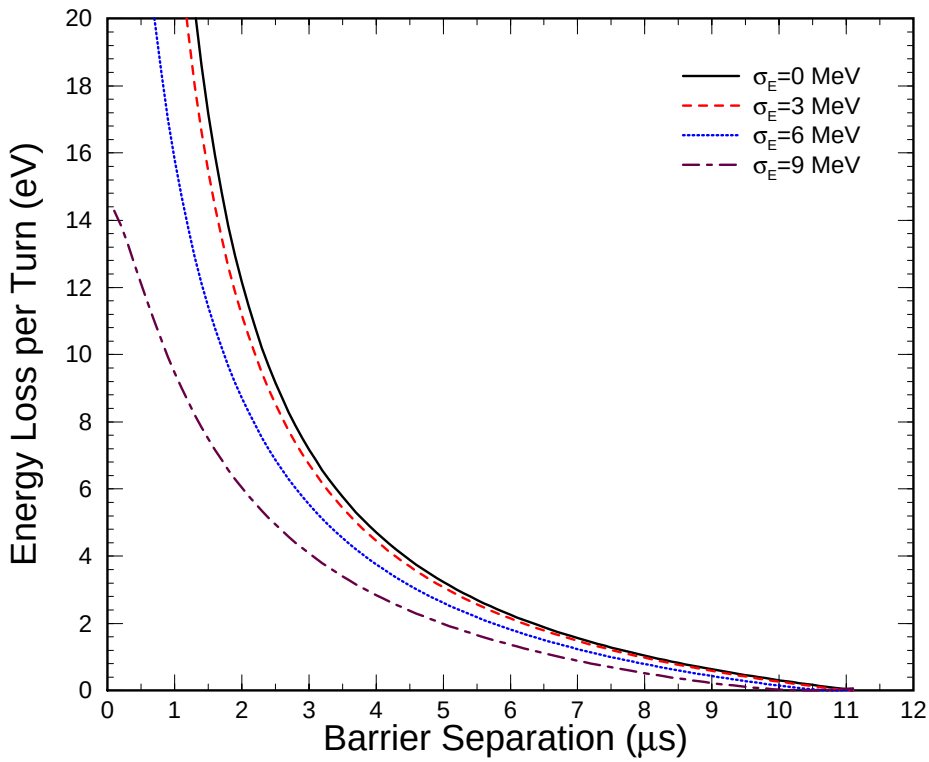

Figure 6: Total coherent energy loss of a particle per turn of a beam in a barrier bucket is shown as functions of barrier separation τ_0 for rms energy spreads $\sigma_E = 0$, 3, 6, and 9 MeV. The impedance includes contributions from 4 rf cavities, 2 resistive-wall monitors, and the resistive wall of the beam pipes. Discrete summation over harmonics has been employed.

As a last remark, we would like to point out that the low-frequency part of the longitudinal impedance of the vacuum chamber contributes only to the parasitic energy loss. We will show in below that the longitudinal impedance in this frequency region will not drive any coherent instabilities. The instability growth rate is usually proportional to the summation of the power spectrum of the beam multiplied by $\mathcal{R}e\, Z_0^{\|}/\omega$, or

$$\text{Growth rate} \propto \sum_{n=-\infty}^{\infty} h_m(n\omega_0 + m\omega_s) \frac{\mathcal{R}e\, Z_0^{\|}(n\omega_0 + m\omega_s)}{n\omega_0 + m\omega_s} \ , \tag{4.5}$$

where $h_m(\omega)$ represents the power spectrum of the mth azimuthal mode of longitudinal oscillation. Notice that $h_m(\omega)$ and $\mathcal{R}e\, Z_0^{\|}(\omega)$ are both symmetric function of ω. The summation therefore vanishes in the absence of the synchrotron frequency $\omega_s/(2\pi)$. Thus, the beam can be unstable only in the presence of synchrotron oscillation. This is the Robinson type of instability derived from the difference in $\mathcal{R}e\, Z_0^{\|}$ at the upper and lower synchrotron sidebands of a revolution harmonic. Since the Recycler beam is confined between two barrier waves,

synchrotron oscillation is extremely slow. If we neglect the time a beam particle spends inside the barrier waves, the synchrotron tune can be estimated easily. For each turn, a particle with rms energy spread σ_E has the arrival time slip $\Delta T = |\eta|\sigma_E T_0/(\beta^2 E)$. For time separation τ_0 between the barriers, the number of revolution turns for the particle to slip through the rf-voltage-free length is $2\tau_0/\Delta T$. Thus the rms synchrotron tune is

$$\nu_s\Big|_{\rm rms} \leq \frac{\Delta T}{2\tau_0} = \frac{|\eta|\sigma_E T_0}{2\beta^2 E\tau_0} \ , \tag{4.6}$$

where the equality sign holds when the barrier voltages are $\pm\infty$. For a beam with barrier separation $\tau_0 = 1$ μs and rms energy spread $\sigma_E = 3$ MeV, $\nu_s\big|_{\rm rms} \leq 1.6 \times 10^{-5}$. Thus, we should not anticipate any sizable growth rate for the Robinson type of instability.

There can still be instabilities when the azimuthal mode number m can no longer classify the modes. This happens when the coherent shifts of the modes are large enough that two modes meet with each other. Since these azimuthal modes are separated by the synchrotron frequency in the absence of the driving impedance, one may think it would be easy for two modes to meet because the synchrotron tune is tiny. An estimate of the threshold can be obtained when the shift is of the order of the synchrotron frequency ($\nu_s \sim \sqrt{6}\nu_s\big|_{\rm rms}$). This leads to the stability condition [4]

$$\frac{\mathcal{I}m\, Z_0^{\parallel}}{n}\bigg|_{\rm eff} \lesssim \frac{3\beta^2 E\nu_s^2\omega_0^3\tau_0^3}{4\pi^2|\eta|eI_{\rm av}} = 9\pi\frac{|\eta|E}{eI_{\rm local}\beta^2}\left(\frac{\sigma_E}{E}\right)^2 \ , \tag{4.7}$$

where $I_{\rm local} \sim I_{\rm av}T_0/\tau_0$ is the local beam current, $I_{\rm av} = eNf_0$ is the average beam current, and Eq. (4.6) has been used. For the 100×10^{10} beam with separation $\tau_0 = 1$ μs between the barriers at rms energy spread $\sigma_E = 3$ MeV, we obtain $\mathcal{I}m\, Z_0^{\parallel}/n\big|_{\rm eff} \lesssim 1530\ \Omega$. On the other hand, the effective impedance is defined as

$$\frac{\mathcal{I}m\, Z_0^{\parallel}}{n}\bigg|_{\rm eff} = \frac{\displaystyle\sum_{n=-\infty}^{\infty}\frac{\mathcal{I}m\, Z_0^{\parallel}}{n}h_m(n\omega_0 + m\omega_s)}{\displaystyle\sum_{n=-\infty}^{\infty}h_m(n\omega_0 + m\omega_s)} \ . \tag{4.8}$$

If we used the representation of impedance in Eq. (3.2), with $R_{\rm gap} = 26\ \Omega$ and $\omega_r/(2\pi) =$ 3 kHz for the resistive wall monitors, and $R_{\rm gap} = 209\ \Omega$ and $\omega_r/(2\pi) = 50$ kHz for the four rf cavities, it is obvious that the Recycler Ring is very much below this stability limit. In fact, no longitudinal coupled-mode instabilities have ever been reported in any hadron machine.

Since the synchrotron frequency is so low, the barrier-confined beam resembles a coasting beam. Another possible instability is the classical microwave instability. The stability limit can be estimated using a Keil-Schnell-like criterion derived by Wang, [5]

$$\frac{\left|Z_0^{\parallel}\right|}{n} \lesssim \frac{2\pi|\eta|E}{eI_{\rm local}\beta^2}\left(\frac{\sigma_{_E}}{E}\right)^2 \ . \tag{4.9}$$

For the above beam, this gives $\left|Z_0^{\parallel}\right|/n \lesssim 400\ \Omega$. The estimated longitudinal impedance is very much less than this limit.

ACKNOWLEDGMENT

The author would like to thank Drs. J. Crisp, Z. Qian, and D. Wildman for some very valuable discussions.

References

[1] A. Hofmann and T. Risselada, *Measuring the ISR Impedance at Very High Frequencies by Observing the Energy Loss of a Coasting Beam*, IEEE Trans. Nucl. Sc., **NS-30**, No. 4, 2400 (1983). J. Arnold, et al, *Energy Loss of proton and Lead Beams in the CERN-SPS*, PAC'97, p.1813.

[2] J.E. Dey and D.W. Wildman, *Wideband Rf System for the Fermilab Recycler Ring*, PAC'99, New York, 1999, p.869.

[3] C.M. Bhat and K.Y. Ng, *Potential-Well Distortion in Barrier RF*, Proceedings of the 30th Advanced ICFA Beam Dynamics Workshop on High Luminosity e+e- Collisions, October 13 - 16, 2003 Stanford, California.

[4] See for example, A.W. Chao, *Physics of Collective Beam Instabilities in High Energy Accelerators*, Wiley-Interscience, 1993.

[5] S. Krinsky and J.M. Wang, Particle Accelerators **17**, 109 (1985).